Check for updates

Solar RRL

RESEARCH ARTICLE

Unshaded Regions Contribute 4–12× Higher Module-Level Reverse-Bias Current Density than Shaded Regions in Partially Shaded Solar Cells Revealed by a Physically Interpretable Model

Yingfeng Li[1] | Zhihan Liu[1] | Keyu Jiang[1] | Peici Yu[1] | Jiaqi Liu[1] | Yunbing Liu[2] | Zhou Cheng[2] | Meicheng Li[1]

[1]State Key Laboratory of Alternate Electrical Power System with Renewable, Energy Sources, School of New Energy, North China Electric Power University, Beijing, China | [2]Gui'an Power Supply Bureau, Guizhou Power Grid Corp., Guiyang, China

Correspondence: Yingfeng Li (liyingfeng@ncepu.edu.cn) | Meicheng Li (mcli@ncepu.edu.cn)

Received: 11 January 2026 | **Revised:** 22 March 2026 | **Accepted:** 26 March 2026

Keywords: avalanche current | avalanche multiplication effect | partial shading | photovoltaic module

ABSTRACT

Partial shading forces the affected cell in a photovoltaic module to operate under reverse bias,resulting in a module-level reverse-bias current. This reverse-bias is widely recognized as the direct physical origin of hotspots formation in photovoltaic (PV) modules, and severe hotspots can lead to irreversible degradation of PV modules. Existing breakdown-extended models typically treat a partially shaded cell as a homogeneous unit, obscuring the respective contributions of shaded and unshaded regions within the same cell. In this study, a physically interpretable dual-region equivalent-circuit model for a shaded cell was constructed based on the mechanism of the avalanche multiplication effect. In the model, avalanche multiplication in the shaded region is driven primarily by leakage current, whereas in the unshaded region it is driven by both leakage current and photogenerated current. Based on the measured *I–V* characteristic data under different shading ratios, the model parameters are determined via numerical fitting with clear physical meaning. The results show that the unshaded region contributes approximately 4–12 times higher module-level reverse-bias current density than the shaded region. This study provides a mechanistic framework for analyzing module operation under partial shading and interpreting reverse-bias behavior in terms of region-resolved contributions.

1 | Introduction

Photovoltaic (PV) technology is expected to become the dominant source of electricity generation, driven by the abundance of solar resources and its advantages as a clean, renewable, and cost-effective energy solution [1, 2]. Solar energy, the fastest-growing source of electricity generation for the 19th year, is leading the energy revolution. By 2023, solar PV alone accounted for approximately 35% of the world's clean installed capacity. In fact, solar PV capacity additions surged by over 80% in 2023, setting a new record of 425 GW [3]. Solar PV reached a 5.5% share of the global electricity mix in 2022, and according to the prediction of the International Energy Agency (IEA), by 2050, solar will account for approximately 41% of global electricity demand [4].

Centralized PV power generation and distributed PV power generation represent two distinct approaches to the development of PV energy systems. Centralized PV power stations are mainly constructed in remote or nonresidential areas. Distributed PV systems are typically located on rooftops, including those of residential, commercial, and industrial locations [5–9].

In the recent 2 years, distributed solar PV accounted for about half of total solar PV capacity additions [10]. Compared with centralized PV, distributed PV offers benefits such as installation-flexibility, maintenance-ease, and operation-independence;

Yingfeng Li, Zhihan Liu contributed equally to this work and are co–first authors.

© 2026 Wiley-VCH GmbH.

however, the operating environment of distributed PV systems is also more complex. PV modules are sometimes shaded by nearby buildings, trees, or other structures [11], and in some cases, they may be covered by leaves, bird droppings, or accumulated dust [12, 13], as illustrated in Figure 1a. When shaded, the output power of the affected PV modules is significantly reduced [14]. This will lead to a mismatch in the operation of the PV array, resulting in hotspot effects, which shorten the lifespan of the modules [15], and in severe cases, may even trigger fires [16].

To date, numerous studies have explored the output characteristics of PV modules under partial shading conditions. These investigations consistently demonstrate that the actual power loss of PV modules under partial shading is significantly lower than the theoretical power loss estimated based on the shading ratio. For instance, M.C. Alonso-García et al. reported that when a single cell in a series-connected module is half-shaded, the module's maximum power loss is 32%, while full shading of the cell results in a maximum power loss of 79%, which are 18% and 21% lower than the theoretical values, respectively [17]. Similarly, Alberto Dolara et al. observed that when a single cell in a module comprising two cell strings arranged in parallel is fully shaded, the module's power loss is 31%, reflecting a 19% reduction compared to the theoretical estimate (50%) [18]. The underlying reason for this phenomenon is that a cell shaded by external factors has to bear a reverse-bias created by other parts exposed to sunlight. This reverse-bias generates a reverse-bias current in the shaded cell that flows in the same direction as the photocurrent, thereby mitigating the adverse impact of partial shading on the overall performance of the PV module.

Volker et al. introduced an extension term to account for diode breakdown and developed a model capable of reproducing the *I–V* characteristics of PV modules under partial shading [19]. Their results showed that shading 75% of a cell, corresponding to only about 2% of the total module area, could still cause a power loss as high as 70%. Even with a bypass diode spanning 18 cells, the loss was only reduced to 55%, indicating that partial shading can induce performance degradation far disproportionate to the shaded area. The significance of this work lies in incorporating reverse-breakdown behavior into the simulation framework of shaded PV modules. A limitation of this model is that it treats the shaded cell as a whole and does not distinguish the different contributions of the shaded and unshaded parts to the module reverse current, making it difficult to reveal the detailed mechanisms of reverse-current formation and hotspot development under partial shading.

To address this issue, unlike the work of Volker et al., which treats a partially shaded cell as an integral whole, our study develops a power-generation characteristic model for partially shaded PV module, aiming to clarify the formation mechanism of reverse current and improve the physical meaning of the model parameters under partial shading conditions. The core of this model is the explicit recognition that, under partial shading, the unshaded region of the cell is also under reverse bias and that its reverse-bias voltage can induce an additional current. On this basis, separate current expressions are established in the equivalent model for the shaded region and the unshaded region, and these two contributions are treated as parallel branches that together constitute the reverse-bias current term of a partially shaded PV module, thereby enabling a separated description of the contributions from different regions within a partially shaded cell. Furthermore, by adjusting the shading ratio and measuring the corresponding *I–V* data, the parameters of the proposed theoretical model were fitted and validated. Compared with existing models that can only reproduce the overall output characteristics of a module under partial shading, the present model can further reveal the different contributions of the shaded and unshaded regions to the reverse current, thereby improving the physical interpretability and engineering applicability of the model parameters.

2 | Experimental Details and Research Process

The PV module used in this study is a crystalline silicon PERC module comprising 36 cells connected in series with a bypass diode in parallel. The nominal parameters of the module are as follows: $P_{max} = 100$ W, $V_{oc} = 18$ V, and $I_{sc} = 6.66$ A. The

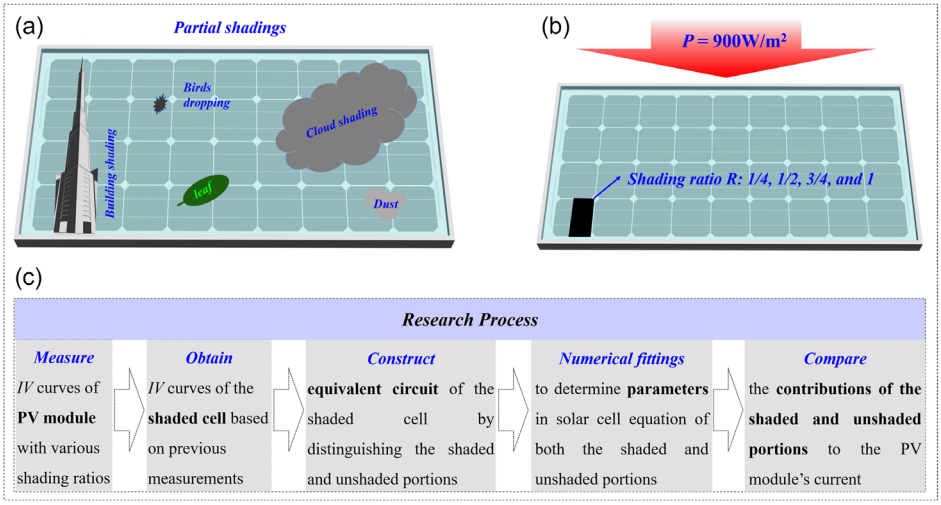


FIGURE 1 | (a) Common shading scenarios in distributed photovoltaics. (b) Simulation method for partially shading. (c) Research process in this work.

ambient temperature during the experiments was 20°C (±1°C). Solar irradiance incident on the module was measured using a solar irradiance meter from Lailx Technology. To ensure consistent conditions, the module's tilt angle was adjusted to maintain a fixed irradiance of 900 W/m^2.

Opaque materials with zero transmittance were affixed to the PV glass to simulate partial shading conditions (as demonstrated in Figure 1b). The shading ratios for a single cell were systematically set to 0, 1/4, 1/2, 3/4, and 1. An *I–V* testing platform for the PV module was constructed using a DC electronic load (ITECH IT8813B) and a data acquisition system (ITECH IT9380) to scan the *I–V* curves of the module under various shading conditions.

This study aims to determine the contributions of the shaded and unshaded regions within a partially shaded cell in a PV module by investigating their I–V characteristics individually and performing numerical fittings. The research process, as illustrated in Figure 1c, consists of five steps. *Step 1*: Measure the *I–V* curves of the PV module under various shading ratios. *Step 2*: Obtain the *I–V* characteristics of the shaded cell based on the previous measurements and establish the relationship between the reverse-bias voltage of the shaded cell, the module's voltage, and the shading ratio. *Step 3*: Develop an equivalent circuit model and the solar cell equation for the shaded cell by distinguishing the shaded and unshaded portions within the same cell. *Step 4*: Determine the parameters in the solar cell equation for both the shaded and unshaded portions through numerical fitting, as well as the parameters in the relationship between the reverse-bias voltage of the shaded cell, the module voltage, and the shading ratio. *Step 5*: Based on the proposed model and parameters, compare and analyze the contributions of the shaded and unshaded portions to the current of the PV module and examine the impact of partial shading on the short-circuit current and fill factor of the PV module.

3 | Results and Discussion

3.1 | Much Larger Current than Expected and Explanation

We initially measured the *I–V* curves of the PV module under various partial shading ratios, as shown in Figure 2. These curves exhibit characteristics consistent with those reported in the literature [19]. For comparison, we also present the theoretical *I–V* curves of the module for each shading ratio in Figure 2, calculated using a simplified series-parallel model, which does not account for the reverse-bias current. The theoretical current is calculated as the product of the unshaded ratio, 1-*R*, and the current of the unshaded module, that is, $\boldsymbol{I}_{\mathrm{Theo}} = (1 - R) \times I_{\mathrm{unshaded}}$.

It can be clearly observed that, under various partial shading ratios, the actual output current, I_{Meas}, is significantly higher than I_{Theo}. This difference is especially pronounced when the PV module is short-circuited. To facilitate the description, we define a quantity ΔI_{sc} to describe the difference between the measured short-circuit current, $I_{\mathrm{sc\text{-}Meas}}$, and the theoretical short-circuit current, $I_{\mathrm{sc\text{-}Theo}}$, where $\Delta I_{\mathrm{sc}} = I_{\mathrm{sc\text{-}Meas}} - I_{\mathrm{sc\text{-}Theo}}$, as also indicated in Figure 2. The values of $I_{\mathrm{sc\text{-}Meas}}$, $I_{\mathrm{sc\text{-}Theo}}$, and ΔI_{sc} under various shading ratios are provided in Table 1.

This additional current, ΔI_{sc}, can be attributed to the reverse-bias current generated in the shaded cell. The reverse-bias current includes the leakage-current related to the shunt resistance, the reverse-bias-current of an ideal p–n junction, and the breakdown current across the junction. As illustrated in Figure 3a, the PV module can be divided into two parts: a single shaded cell and the remaining 35 unshaded cells. For ease of description, they are referred to as "1-cell" and "35-cells", respectively. These two parts are connected in series, which imposes a constraint that the current through the shaded cell must equal that through the

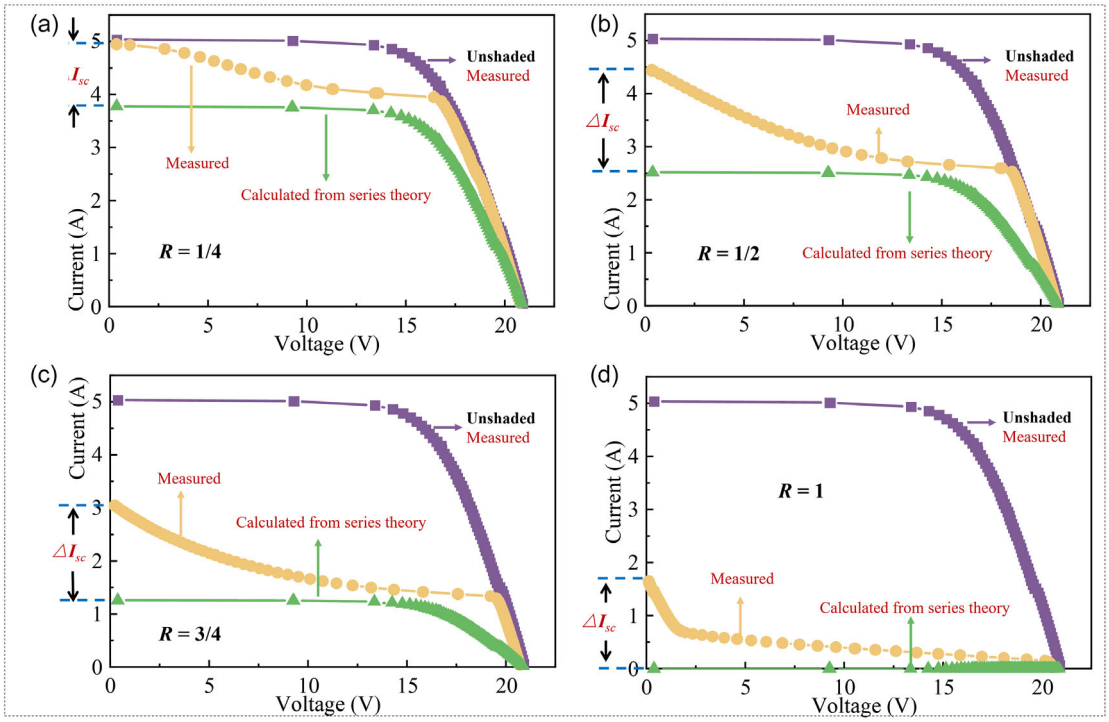


FIGURE 2 | Comparison between measured and theoretical *I–V* curves of PV module under various shading ratios. (a) $R = 1/4$. (b) $R = 1/2$. (c) $R = 3/4$. (d) $R = 1$. For reference, *I–V* curves of the unshaded module were also given.

TABLE 1 | Short-circuit current and open-circuit voltage of PV module under varying shading ratios.

R	$I_{sc\text{-}Meas}$, A	$I_{sc\text{-}Theo}$, A	ΔI_{sc}, A	V_{OC}, V
0	5.037	—	0	20.869
1/4	4.952	3.778	1.174	20.773
1/2	4.453	2.519	1.934	20.781
3/4	3.049	1.259	1.790	20.714
1	1.650	0	1.650	20.524

unshaded cells. As a result, the current generated by "35-cells" is "blocked" by "1-cell", leading to charges accumulation at the cell's terminals. This accumulation subjects "1-cell" to a reverse-bias voltage, which induces a reverse-bias current in "1-cell" flowing in the same direction as the photocurrent, $I_{ph\text{-}shad}$. When the reverse-bias voltage becomes sufficiently high, it can even trigger an avalanche multiplication effect in "1-cell". However, the magnitude of the reverse-bias current during avalanche breakdown is limited by the short circuit current of the unshaded module and, therefore, will not become excessively large.

The *I–V* curves of "1-cell" (with $R = 0$, 1/2, and 1) and "35-cells" are shown in Figure 3b, represented by dashed and solid lines, respectively. When $R = 0$, the operating state of "1-cell" (black dashed line) is identical to that of "35-cells", except that its output voltage is 1/35 of the output voltage of "35-cells". However, when $R \neq 0$, the *I–V* curves of "1-cell" become more complex. If the load resistance of the module is sufficiently large, such that the output current of "35-cells" is less than the maximum photocurrent $I_{sc} \times (1-R)$ that "1-cell" can generate, "1-cell" operates in a forward-biased state, represented by the dashed line on the right side of the axes. As the load resistance decreases, "1-cell" begins to limit the module's current, causing it to suffer from reverse-bias. The smaller the load resistance, the closer the module operates to short-circuit conditions, making the current limitation imposed by "1-cell" more pronounced. Consequently, the reverse-bias voltage (V_{rev}) experienced by "1-cell" increases. V_{rev} drives a reverse-bias current (I_{rev}) in "1-cell", which flows in the same direction as the photocurrent. As V_{rev} increases, the avalanche multiplication effects occur, leading to a rapid rise in I_{rev} within "1-cell", as shown by the dashed lines on the left side of the axes. According to the aforementioned constraint, the sum of the $I_{sc} \times (1-R)$ and I_{rev} in "1-cell" must equal the current of "35-cells". Therefore, the intersections of the horizontal dashed lines with the *I–V* curves represent the operating states of "1-cell" and "35-cells" at a given module output current. When the module operates under short-circuit conditions, the V_{rev} experienced by "1-cell" equals the voltage of "35-cells", and the current of "1-cell" reaches the maximum value: the short-circuit current of the module.

From Table 1, it can also be observed that the change in ΔI_{sc} shows a trend of initially increasing and then decreasing with the increase in R of "1-cell", reaching a maximum of 1.934 A at $R = 1/2$. This indicates that the shaded and unshaded portions of "1-cell" contribute differently to I_{rev}, with the unshaded portion providing a larger I_{rev}. This is because the unshaded portion has a higher carrier concentration (photogenerated carriers), resulting in a more significant avalanche multiplication effect compared to the shaded portion. When $R < 1/2$, the increase in ΔI_{sc} with R can be attributed to the gradually increasing V_{rev}. However, when $R > 1/2$, the decrease in ΔI_{sc} with R can be explained by the reduced area of the unshaded portion. A detailed comparison of the contributions of the shaded and unshaded portions to I_{rev} will be provided in subsequent sections.

3.2 | *I–V* Characteristics of the Shaded Cell

The *I–V* characteristics and operational mechanisms of a PV module under partial shading are primarily determined by those of the shaded cell. Therefore, in this section, we derive the *I–V* characteristics of the shaded cell by analyzing the data in Figure 2 (the *I–V* characteristics of the module), which will serve as the foundation for investigating the module's operational mechanisms.

Initially, the relationship between the reverse-bias current of the shaded cell (I_{rev}) and the voltage of the entire module (V_{module}) was determined using the method illustrated in Figure 4a, resulting in the I_{rev}-V_{module} curves. Each point on the module's *I–V* curve provides the values of V_{module} and the corresponding current (I) flowing through the module. The current I consists of two components: the photocurrent of the shaded cell ($I_{ph\text{-}shad}$) and I_{rev}. Here, $I_{ph\text{-}shad}$ is constant for a given shading ratio, equal to $I_{sc\text{-}Theo}$ as presented in Column 2 of Table 1. By subtracting $I_{ph\text{-}shad}$ from I, I_{rev} can be calculated. The resulting I_{rev}-V_{module} curves are depicted in Figure 4b. It can be observed that I_{rev} decreases as V_{module} increases. When V_{module} is sufficiently high, I_{rev} gradually decreases to zero, corresponding to the scenario where the voltage across the shaded cell is zero. As V_{module} increases further, the shaded cell transitions to a forward-biased state, and the shape of the I_{rev}-V_{module} curve is governed by the characteristics of a p–n junction under forward-bias. The V_{module}

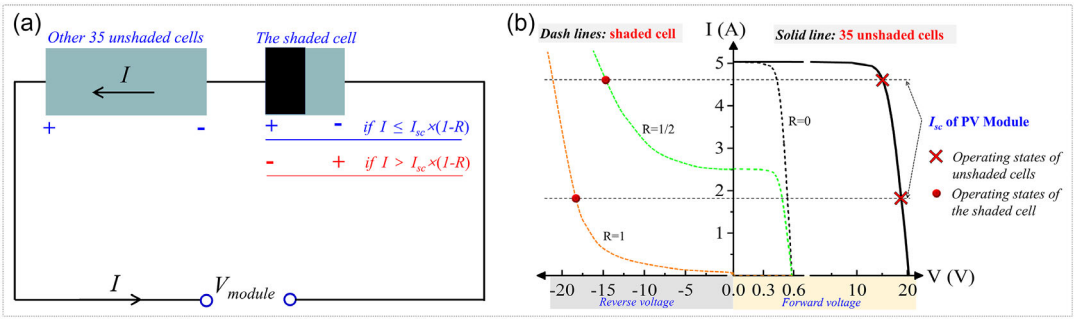


FIGURE 3 | (a) The equivalent circuit diagram of a PV module with one cell shaded. (b) The *I–V* curves of the shaded cell and the remaining 35 unshaded cells under various shading ratios.

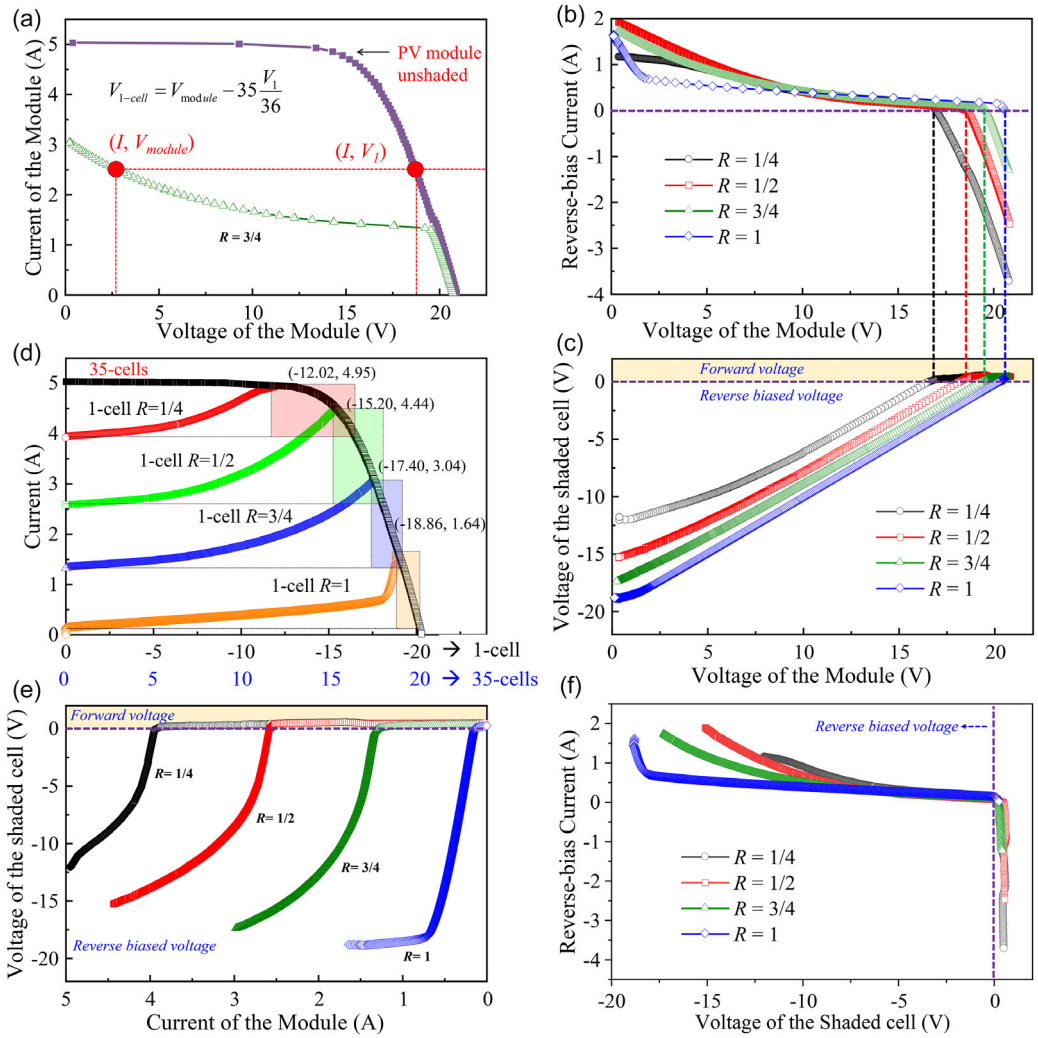


FIGURE 4 | (a) Method for determining the voltage of the shaded cell. (b) Relationship between the dark current of the shaded cell and the voltage of the module, under various shading ratios. (c) Relationship between the voltage of the shaded cell and the voltage of the module, under various shading ratios. (d) *I–V* curves of the shaded cell and the remaining 35 unshaded cells, under various shading ratios, when the shaded cell is in reverse bias. (e) Relationship between the voltage of the shaded cell and the module current, under various shading ratios. (f) Relationship between the reverse-bias current and voltage of the shaded cell under various shading ratios.

values at which the shaded cell transitions from reverse-bias to forward-bias vary under different shading ratios. For shading ratios of 1/4, 1/2, 3/4, and 1, the V_{module} values corresponding to $I_{\text{rev}} = 0$ are 16.97, 18.58, 19.59, and 20.60 V, respectively.

Next, the relationship between the voltage across the shaded cell ($V_{1\text{-cell}}$) and V_{module} was determined. As shown in Figure 4a, by drawing a horizontal line from the point (I, V_{module}), an intersection with the *I–V* curve of the unshaded module can be obtained. The voltage at this intersection, V_1, corresponds to the output voltage of the unshaded module (composed of 36 cells) when the output current is I. Under shaded conditions, the 35 unshaded cells within the module operate in the same state as the cells in the unshaded module, with a current–voltage characteristic of I, $V_1/36$. Therefore, the total voltage provided by the 35 unshaded cells can be expressed as: $V_{35\text{-cells}} = V_1 \times 35/36$. The voltage across the shaded cell, $V_{1\text{-cell}}$, can then be calculated as: $V_{1\text{-cell}} = V_{\text{module}} - V_1 \times 35/36$. The relationship between $V_{1\text{-cell}}$ and V_{module} is illustrated in Figure 4c. It can be observed that when V_{module} is relatively low, the shaded cell operates in a reverse-biased state, with the reverse bias increasing as V_{module} decreases. When V_{module} exceeds a certain threshold, the shaded cell transitions to a forward-biased state. The points where $V_{1\text{-cell}} = 0$ correspond to the module voltages at which $I_{\text{rev}} = 0$, as indicated by the dashed lines in Figure 4.

Based on the above analysis, we obtained the *I–V* characteristics of the shaded cell in its reverse-biased state (the right half of Figure 3b), which are plotted in Figure 4d (with the horizontal axis taking negative values). For completeness, the *I–V* characteristics of the 35 unshaded cells are also plotted (with the horizontal axis taking positive values). Under various shading ratios, the actual short-circuit current of the entire module, as shown in Figure 2, corresponds to the intersection points in Figure 4d. For nonshort-circuit conditions, the operating states of "1-cell" and 35 other cells within the module can also be determined from Figure 4d: by drawing a horizontal line with a given current I, the intersection of this line with the colored curve indicates the operating state of 1-cell, while the intersection with the black curve represents the operating state of the 35 unshaded cells. The width

of the colored translucent rectangles in Figure 4d corresponds to the voltage variation range of the 35 unshaded cells under various shading ratios. It can be observed that, compared to the shaded cell, the voltage variation range of the 35 unshaded cells is relatively small. Moreover, the greater the shading ratio, the smaller the voltage variation range of the 35 unshaded cells.

As mentioned above, $V_{1\text{-cell}}$ results from charge accumulation across the cell. Therefore, it is expected to be more sensitive to the module current, I. Figure 4e presents the relationship between $V_{1\text{-cell}}$ and I. It can be observed that the shaded cell remains in a reverse-biased state at high module currents; the larger the current, the greater the reverse-bias voltage. When the module current decreases below a certain threshold, marked by the intersection of the $V_{1\text{-cell}}$-I curves with the line $V_{1\text{-cell}} = 0$, the shaded cell transitions to a forward-biased state. For shading ratios of 1/4, 1/2, 3/4, and 1, the module currents at this transition point are 3.92, 2.59, 1.28, and 0.14 A, respectively. These values correspond to the photocurrents of the shaded cell, as listed in Column 2 of Table 1. As shown in Figure 4e, when the shaded cell is in a reverse-biased state, $V_{1\text{-cell}}$ is indeed highly sensitive to variations in the module current.

The key mechanism behind the generation of I_{rev} in the shaded cell can be directly reflected by the relationship between I_{rev} and $V_{1\text{-cell}}$, as illustrated in Figure 4f. Under full shading conditions, a distinct inflection point appears on the I_{rev}-$V_{1\text{-cell}}$ curve when $V_{1\text{-cell}} = -18.2$ V. This indicates that when the reverse-bias voltage exceeds 18.2 V, the reverse-bias current of the cell increases significantly. According to semiconductor theory, when the reverse-bias voltage across a silicon p–n junction reaches a critical value, avalanche multiplication occurs [20]; and the avalanche breakdown voltage is around 18 V when the doping concentration of approximately 8×10^{16} on the lightly doped side. Additionally, Xu also reports that the avalanche breakdown voltage for solar cells in the dark is approximately 18 V [21]. Therefore, the inflection point can be rationally explained by the occurrence of significant avalanche multiplication within the solar cell. Meanwhile, the actual avalanche breakdown voltage should be slightly greater than 18 V, as avalanche breakdown is defined by an infinite reverse current at the breakdown voltage. To the right of the inflection point, the reverse-bias current does not remain constant but instead increases approximately linearly with voltage. This behavior indicates the presence of leakage current in the solar cell, which corresponds to a finite shunt resistance. From Figure 4f, a decrease in the shading ratio leads to a significant increase in the reverse-bias current under the same reverse-bias voltage. This observation demonstrates that the shaded and unshaded portions of the module contribute differently to the reverse-bias current, with the unshaded portion making a larger contribution.

3.3 | Solar Cell Equation Distinguishing the Shaded and Unshaded Portions

In the previous sections, the I–V characteristics of the shaded cell have been extracted and analyzed. In this section, we build the equivalent circuit and solar cell equation for the shaded cell based on the previous conclusions. The equivalent circuit is shown in Figure 5a, where the shaded and unshaded portions are distinguished and connected in parallel [22]. I and $V_{1\text{-cell}}$ represent the total current and voltage of the shaded cell, respectively. I_{ph} is the

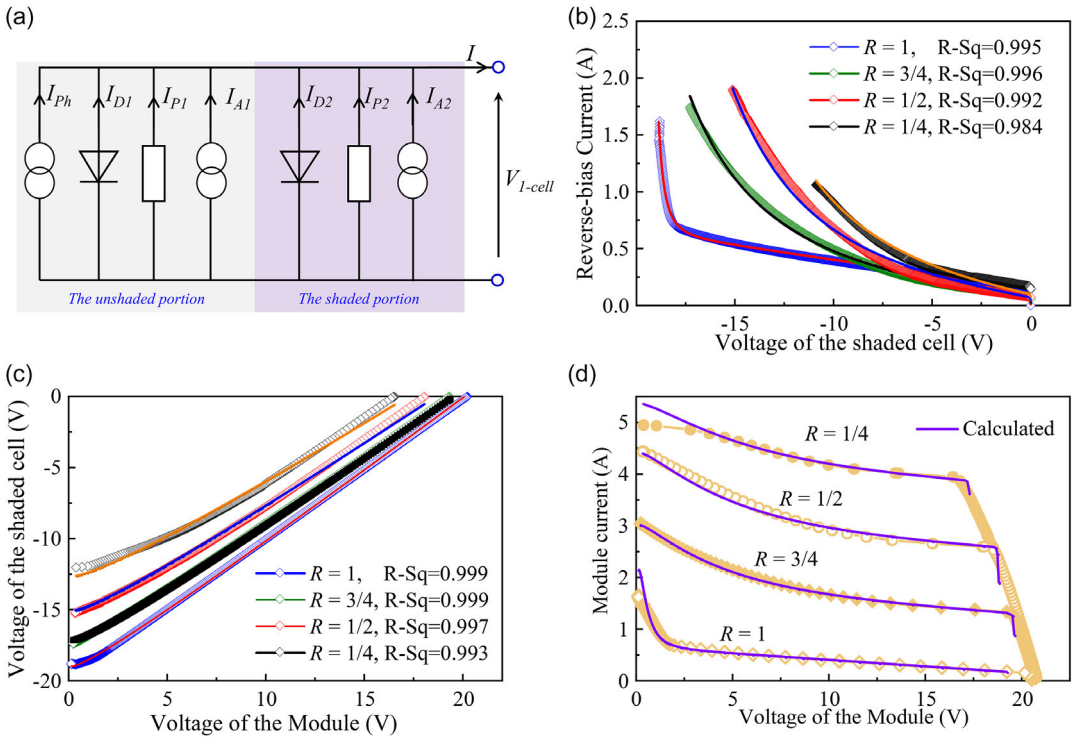


FIGURE 5 | (a) Equivalent circuit of the partially shaded solar cell in the PV module. The unshaded portion contributes the photogenerated current I_{ph}, a diode reverse-bias current I_{D1}, a leaky current corresponding to the shunt resistance I_{P1}, and an avalanche current I_{A1}; while, the shaded portion contributes I_{D2}, I_{P2}, and I_{A2}. (b) Comparison between measurements and numerical fitting of the I_{rev}-$V_{1\text{-cell}}$ curves under different shading ratios. (c) Comparison between measurements and numerical fitting of the $V_{1\text{-cell}}$-V_{module} curves of the shaded cell under different shading ratios. (d) Calculated I–V curves using the proposed solar cell equations comparing with the measured results, under various shading ratios.

photocurrent of the unshaded portion, given by $I_{ph} = (1\text{-}R) \times I_{sc}$. I_{P1} and I_{P2} denote the leakage currents associated with the shunt resistance for the unshaded and shaded portions, respectively. I_{D1} and I_{D2} represent the reverse-bias currents for the ideal p–n junction of the unshaded and shaded portions, respectively. I_{A1} and I_{A2} correspond to the avalanche breakdown currents for the unshaded and shaded portions, respectively.

Based on the model proposed in Figure 5a, the equation for the reverse-bias current, $I_{rev} = I - I_{ph}$, of the shaded cell can be written as,

$$\begin{aligned} I_{rev} = I - I_{Ph} &= I_{rev-shaded} + \Delta I_{rev-unshaded} \\ &= R * I_s \left[\exp\left(\frac{qV_{1-cell}}{mk_BT}\right) - 1 \right] \\ &+ R * \frac{V_{1-cell}}{R_P} + R * \frac{V_{1-cell}}{R_P} a \left(1 - \frac{V_{1-cell}}{V_{Br,1}}\right)^{-n1} \\ &+ (1-R) * I_s * \left[\exp\left(\frac{qV_{1-cell}}{mk_BT}\right) - 1 \right] \\ &+ (1-R) * \frac{V_{1-cell}}{R_P} + (1-R) * \frac{V_{1-cell}}{R_P} \\ &* b \left(1 - \frac{V_{1-cell}}{V_{Br,2}}\right)^{-n2} + (1-R) * I_{ph} \\ &* b \left(1 - \frac{V_{1-cell}}{V_{Br,2}}\right)^{-n2} \end{aligned} \tag{1}$$

$I_{rev\text{-}shaded}$ and $I_{rev\text{-}unshaded}$ represent the contributions to I_{rev} from the shaded and unshaded portions, respectively, Among which:

$$\begin{aligned} I_{rev-shaded} &= I_{D2} + I_{P2} + I_{A2} \\ &= R * I_s \left[\exp\left(\frac{qV_{1-cell}}{mk_BT}\right) - 1 \right] \\ &+ R * \frac{V_{1-cell}}{R_P} + R * \frac{V_{1-cell}}{R_P} a \left(1 - \frac{V_{1-cell}}{V_{Br,1}}\right)^{-n1} \end{aligned} \tag{2}$$

The first term represents the reverse current of the ideal p–n junction, which is very small. Here, R is the shading ratio, I_s is the reverse saturation current of the shaded cell, and m is the ideality factor. The second term represents the reverse ohmic current, where R_p is the equivalent shunt resistance of the shaded cell. The third term corresponds to the reverse-bias current caused by the avalanche effect, where it is assumed that the avalanche multiplication is primarily triggered by the reverse ohmic current associated with the shunt resistance [19]. a represents the fraction of the ohmic current involved in the avalanche breakdown, $V_{Br,1}$ is the junction breakdown voltage in the dark, and $n1$ is the avalanche breakdown exponent in the dark, which in ideal conditions is approximately 4 [21].

According to the semiconductor theory [20], the mechanism of the avalanche multiplication effect is as follows: the charge carriers gain energy from the reverse-bias electric field, then collide with electrons in the atoms of the depletion region, generating new electron–hole pairs; this chain reaction continues, leading to the avalanche multiplication effect. Therefore, the photocurrent I_{ph} flowing through the depletion region can be imparted with energy and serve as the trigger current for the avalanche multiplication effect. Thus, the expression for the reverse-bias current of the unshaded portion $I_{rev\text{-}unshaded}$ should be written as:

$$\begin{aligned} I_{rev-unshaded} &= (1-R) * I_s * \left[\exp\left(\frac{qV_{1-cell}}{mk_BT}\right) - 1 \right] \\ &+ (1-R) * \frac{V_{1-cell}}{R_P} + (1-R) * \frac{V_{1-cell}}{R_P} * b \left(1 - \frac{V_{1-cell}}{V_{Br,2}}\right)^{-n2} \\ &+ (1-R) * I_{ph} * b \left(1 - \frac{V_{1-cell}}{V_{Br,2}}\right)^{-n2} \end{aligned} \tag{3}$$

The fourth term represents the reverse-bias current triggered by the avalanche multiplication effect induced by the photocurrent. Under illuminated condition, the fraction of the reverse ohmic current that triggers the avalanche multiplication effect to the photocurrent should be the same, denoted by the parameter b. $V_{Br,2}$ is the avalanche breakdown voltage under illuminated condition (900 W/m^2), and $n2$ is the avalanche breakdown exponent under illuminated condition.

3.4 | Parameters Fitting of the Solar Cell Equation

In the case of full shading ($R = 1$), the reverse-bias current of the shaded cell can be represented solely by Equation (2), which requires the fewest parameters. Therefore, we first fit the I_{rev}-$V_{1\text{-}cell}$ curve when $R = 1$ to determine the parameters R_p, a, $V_{Br,1}$, and $n1$. The fitting result is shown by the red solid line in Figure 5b, with a coefficient of determination (R-Sq) of 0.995, indicating that Equation (2) can effectively explain the I–V characteristics of the shaded solar cell. The obtained parameters R_p, a, $V_{Br,1}$, and $n1$ were determined to be 39.81 Ω, 3.46×10^{-4}, 19.63 V, and 2.68, respectively, as listed in Table 2.

Next, we fixed the parameters R_p, a, $V_{Br,1}$, and $n1$, and fitted the I_{rev}-$V_{1\text{-}cell}$ curves for three different shading ratios, $R = 3/4$, 1/2, and 1/4, using Equation (1). The fitting results for these ratios are shown in Figure 5b, with R-Sq values of 0.996, 0.992, and 0.984, respectively. The values of the parameters b, $V_{Br,2}$, and $n2$ obtained from the fitting process are listed in Table 2. It is evident that, for various shading ratios, the parameters describing the unshaded portion of the solar cell in the formula remain nearly constant. This suggests that the components of Equation (1), which have clear physical significance, can effectively describe the I–V characteristics of partially shaded solar cells under reverse-bias conditions.

TABLE 2 | Parameters in Equation (1) obtained based on numerical fitting of the I_{rev}-$V_{1\text{-}cell}$ curves in Figure 5b.

R	R_p, Ω	a	$V_{Br,1}$, V	$n1$	b	$V_{Br,2}$, V	$n2$
1	39.81	3.46E-4	19.63	2.68	—	—	—
3/4	39.81	3.46E-4	19.63	2.68	2.39 E-2	41	6.8
1/2	39.81	3.46E-4	19.63	2.68	2.01 E-2	40	7.0
1/4	39.81	3.46E-4	19.63	2.68	2.11 E-2	39	6.9

3.5 | Determine Relationship between $V_{1\text{-Cell}}$ and the Module Voltage Parameters Fitting of the Solar Cell Equation

In practical measurements, the voltage of the shaded cell, $V_{1\text{-cell}}$, cannot be directly obtained. Instead, the voltage of the entire module, V_{module}, and the shading ratio, R, are more readily measured. Therefore, establishing a relationship between $V_{1\text{-cell}}$, V_{module}, and R will greatly facilitate the practical application of Equation (1). To achieve this, we will first determine the functional form of the relationship between $V_{1\text{-cell}}$, V_{module}, and R, and then use numerical fitting to determine the parameters of the equation.

As shown in Figure 4c, the voltage of the shaded cell, $V_{1\text{-cell}}$, exhibits an approximately linear relationship with the module voltage, V_{module}. This dependency is expressed using the following equation

$$V_{1-\text{cell}} = AV_{\text{module}} - - V_{35-\text{cells}} \tag{4}$$

where the parameter A reflects the influence of the series resistance in the PV module. The dependence of $V_{1\text{-cell}}$ on R needs to be incorporated in the $V_{35\text{-cells}}$ term. Since the 35 cells are unshaded, their operating equation satisfies

$$I_{35-\text{cells}} = I_{\text{sc}} - I_0\left[\exp\left(\frac{qV_{35-\text{cells}}}{k_BT}\right) - 1\right] \tag{5}$$

It is evident that $V_{35\text{-cells}}$ is determined by $I_{35\text{-cells}}$, and $I_{35\text{-cells}}$ is constrained by the current of the shaded cell, making it related to R. In the simplest case, that is, when $V_{1\text{-cell}} = 0$, $I_{35\text{-cells}} = I_{\text{sc}} \times (1\text{-}R)$. Under this condition, $V_{35\text{-cells}}$ can be expressed as

$$V_{35-\text{cells}} = 35\frac{k_BT}{q}\ln\left[\frac{I_{\text{sc}}R}{I_0} + 1\right] = 0.91\ln\left[BR + 1\right] \tag{6}$$

where $k_BT/q = 0.026\,\text{V}$ at room temperature. And since the reverse saturation current I_0 of a solar cell is not a constant, we replace I_{sc}/I_0 with a variable parameter B.

When the shaded cell is under reverse-bias, the relationship between $V_{35\text{-cells}}$, V_{module}, and R becomes complex. As discussed above, $I_{35\text{-cells}}$ is primarily contributed by the reverse avalanche current flowing through the shaded cell (excluding the photogenerated current). Conversely, the reverse avalanche current is determined by $V_{1\text{-cell}}$, which equals V_{module} - $V_{35\text{-cells}}$. Therefore, it is impossible to derive a clear analytical formula for the relationship between V_{module} and R. Taking into account that the reverse avalanche current differs between the shaded and unshaded portions, we directly added two terms to Equation (6) to describe the dependence of $V_{35\text{-cells}}$ on V_{module} and R. These terms are in a form similar to that of the avalanche current: the breakdown voltages $V_{Br,1}$ and $V_{Br,2}$ are used to define the range of V_{module}'s influence on $V_{35\text{-cells}}$, while the exponents $n3$ and $n4$ represent the degree of the influence. The resulting formula for $V_{35\text{-cells}}$ is given as follows

$$\begin{aligned} V_{35-\text{cells}} = {} & 0.91\ln\left[BR + 1\right] - CR(V_{\text{module}}/V_{Br,1})^{n_3} \\ & - D(1-R)(V_{\text{module}}/V_{Br,2})^{n_4} \end{aligned} \tag{7}$$

where $V_{Br,1}$ and $V_{Br,2}$, which were determined in the aforementioned fittings, are set to 19.63 V and 40 V, respectively. Combining Equations (4) and (7), the relationship between $V_{1\text{-cell}}$, V_{module}, and R can be expressed as

$$\begin{aligned} V_{1-\text{cell}} = {} & AV_{\text{module}} - 0.91\ln\left[BR + 1\right] + CR\left(\frac{V_{\text{module}}}{19.63}\right)^{n_3} \\ & + D(1-R)\left(\frac{V_{\text{module}}}{40}\right)^{n_4} \end{aligned} \tag{8}$$

Based on the data in Figure 4d, numerical fitting was performed to determine the parameters. The values of A, C, D, $n3$ and $n4$ were determined to be 1.09, −3.07, −13.33, 0.45, and 0.70, respectively. The parameter B varies with the shading ratio, taking values of 9.38E8, 1.61E8, 2.65E7, and 3.77E6 for $R = 1$, 3/4, 1/2, and 1/4, respectively. Furthermore, we fitted the relationship between B and R, and the fitting results show that B can be described as

$$B = 834948.34\exp\left(R/0.14234\right) - 1252524.23 \tag{9}$$

with a coefficient of determination R-Sq = 1. The fitting results of $V_{1\text{-cell}}$-V_{module} for various shading ratios are shown in Figure 5c, with R-Sq = 0.999, 0.999, 0.997, and 0.993, respectively. This demonstrates that Equation (8) effectively captures the relationship between $V_{1\text{-cell}}$, V_{module}, and R.

In the solar cell equations obtained above, i.e., Equations (1) and (8), most of the terms have clear physical meanings, and therefore their forms and corresponding parameters do not change with R. The calculated I–V curves of the PV module under various shading ratios were compared with the measured results presented in Figure 5d. The excellent agreement between the calculated and measured results suggests that, by combining Equations (1) and (8), we can effectively describe and analyze the I–V characteristics of a given PV module without bypass diodes under various shading ratios. Furthermore, this approach enables a detailed understanding of the operating states of both the shaded cell and the unshaded cells, as well as the contributions of the shaded and unshaded portions in the same shaded cell to the module current.

3.6 | Comparison Contributions of the Shaded and Unshaded Portions

Based on the solar cell equations obtained, we compare the contributions of the shaded and unshaded portions to the reverse-bias current I_{rev}. Since the parameters in the equations do not change with the shading ratio R, we take $R = 3/4$ as an example and calculated the reverse-bias current density of the shaded and unshaded portions by $I_{\text{rev-shaded}}/R$ and $I_{\text{rev-unshaded}}/(1\text{-}R)$, respectively. The results are shown in Figure 6. As can be seen, at the same reverse-bias voltage, the reverse-bias current density of the unshaded portion is significantly larger than that of the shaded portion, and the gap increases as the reverse-bias voltage increases. At reverse-bias voltages of 5 V, 10 V, 15 V, and 17 V, the reverse-bias current density of the unshaded portion is approximately 3 times, 4 times, 8 times, and 11.3 times that of the shaded portion, respectively. These results clearly indicate that, for partially shaded cells in a PV module, the unshaded portion provides the dominant reverse-bias current path. Additionally, the photogenerated current itself is also contributed by the unshaded portion. Comprehensively, for partially shaded solar cells, when the

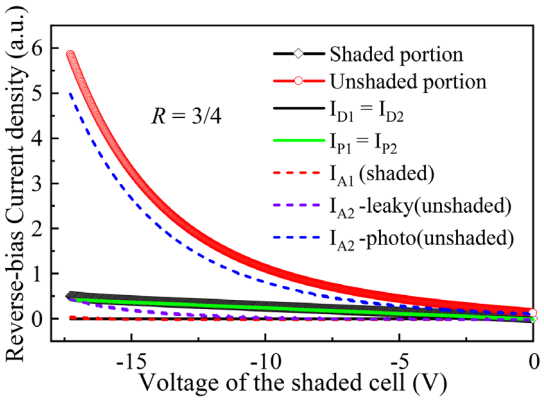


FIGURE 6 | Comparison of the contributions of the shaded and unshaded portions to the reverse-bias current density of the module.

shading ratio is not excessively large, the contribution of the shaded portion can be approximately neglected, and only the contribution of the unshaded portion needs to be considered.

The contributions of each component to the reverse-bias current I_{rev} were also analyzed in detail in Figure 6. It can be observed that the reverse-bias current of the unshaded portion, $I_{rev\text{-}unshaded}$, is primarily contributed by the avalanche current triggered by the photogenerated current, which is much larger than the avalanche current triggered by the reverse Ohmic current. Additionally, the avalanche current induced by the reverse Ohmic current in the unshaded portion is much larger than that in the shaded portion.

4 | Conclusions

Partial shading is a common phenomenon in distributed PV systems. The shaded cell in the module will be in a reverse-biased state, generating a reverse-bias current that flows in the same direction as the photogenerated current. To date, no studies have provided a detailed explanation of the mechanisms behind the reverse-bias current under partial shading conditions, particularly without distinguishing the contributions of the shaded and unshaded portions in the shaded cell.

In this work, the *I–V* characteristics of a PV module with one cell being partially shaded by different ratios ($R = 0$, 1/4, 1/2, 3/4, and 1) were measured. Using the "avalanche breakdown" mechanism, solar cell equations with clear physical significance were constructed for the shaded cells. The established equations distinguish the contributions of the shaded and unshaded regions to the reverse-bias current by introducing the reverse-bias current term triggered by the avalanche multiplication effect induced by the photogenerated current in the unshaded region. Based on the measured *I–V* data, numerical fittings were employed to obtain the parameters of the established equations. All parameters were found to be independent of the shading ratio *R*, ensuring that the solar cell equations we developed have clear physical meaning and good practical applicability. Using these equations, we can accurately and conveniently predict the operating states of the shaded and unshaded cells in the *PV* module, as well as the contributions of the shaded and unshaded portions in the same shaded cell to the overall current of the module, based on the actual shading conditions. Based on the obtained equations, it is demonstrated that the reverse-bias current density of the unshaded portion is approximately 4–12 times that of the shaded portion. Therefore, for cases with relatively small shading ratios, the contribution of the shaded portion of the shaded cell can be approximately neglected, and only the contribution of the unshaded portion needs to be considered. The solar cell equations developed in this paper are of great significance for the qualitative and quantitative analysis of the *I–V* characteristics and operational states of PV modules under partially shading. Combined with the monitoring data, they can provide reliable theoretical and data support for fault detection, operation, and maintenance of photovoltaic systems. However, the study presented here does not account for variations in light intensity and does not consider the impact of bypass diodes, which are commonly installed in PV modules. In future work, we will further investigate the impacts of light intensity and bypass diodes.

Author Contributions

Yingfeng Li: conceptualization, writing – original draft, writing – review and editing, funding acquisition. **Zhihan Liu:** methodology, investigation, data curation, formal analysis, writing – original draft. **Keyu Jiang:** investigation, formal analysis, validation. **Peici Yu:** data curation, validation. **Jiaqi Liu:** data curation, visualization. **Yunbing Liu:** resources, supervision, writing – review and editing. **Zhou Cheng:** methodology, supervision, writing – review and editing. **Meicheng Li:** writing – review and editing, supervision, project administration, funding acquisition.

Acknowledgments

Y. L. and Z. L. contributed equally to this work and are co–first authors. This work was supported partially by the Key Research and Development Program sponsored by the Ministry of Science and Technology (MOST) (grant no. 2022YFB4200301), National Natural Science Foundation of China (grant nos. 52072121, 22409061, 52232008, 52102245, and 52402254), the Beijing Natural Science Foundation (2222076 and 2222077), the Beijing Nova Program (20220484016), Young Elite Scientists Sponsorship Program by CAST (2022QNRC001), 2022 Strategic Research Key Project of Science and Technology Commission of the Ministry of Education, the State Key Laboratory of Alternate Electrical Power System with Renewable Energy Sources (LAPS2024−05), the Fundamental Research Funds for the Central Universities (2022MS029, 2022MS02, 2022MS031, 2023MS042, and 2023MS047) and the NCEPU "Double First-Class" Program.

Funding

This work was supported by the National Natural Science Foundation of China (52072121, 22409061, 52232008, 52102245, 52402254); the beijing natural science foundation (2222076, 2222077); the Beijing Nova Program (20220484016); Young Elite Scientists Sponsorship Program by CAST (2022QNRC001); 2022 Strategic Research Key Project of Science and Technology Commission of the Ministry of Education, the State Key Laboratory of Alternate Electrical Power System with Renewable Energy Sources (LAPS2024−05); Fundamental Research Funds for the Central Universities (2022MS029, 2022MS02, 2022MS031, 2023MS042, 2023MS047); the NCEPU 'Double First-Class' Program; the Key Research and Development Program sponsored by the Ministry of Science and Technology (MOST) (2022YFB4200301).

Conflicts of Interest

The authors declare no conflicts of interest.

Data Availability Statement

The data that support the findings of this study are available from the corresponding author upon reasonable request.

References

1. S. Adak and H. Cangi, "The Quality Problems at Low Irradiance in the Grid-Connected Photovoltaic Systems," *Electrical Engineering* 5 (2024): 6185–6197, https://doi.org/10.1007/s00202-024-02351-6.

2. N. Ameli, F. Nijsse, and J. F. Mercure, *Solar Power Expected to Dominate Electricity Generation by 2050 - even without More Ambitious Climate Policies*, https://theconversation.com/Solar-Power-Expected-to-Dominate-Electricity-Generation-by-2050-even-Without-More-Ambitious-Climate-Policies-215367/; 2023, (2023), accessed 26 October 2023.

3. International Energy Agency,*World Energy Outlook 2024*, (2024), accessed 16 October 2024. https://www.iea.org/reports/world-energy-outlook-2024,

4. U.S. Energy Information Administration. *Annual Energy Outlook 2023*, (2023), accessed November 2023, *Available at:* https://www.eia.gov/outlooks/aeo/data/browser/#/?id=24-AEO2023&region=0-0&cases=ref2023&start=2021&end=2050&f=A&linechart=ref2023-d020623a.4-24-AEO2023~~~~~ref2023-d020623a.30-24-AEO2023&ctype=linechart&sourcekey=0.

5. X. Zhang, K. Yang, C. Shao, and H. Chen, "A Novel Parameterization Scheme for Accurate and Efficient Radiation Transfer Modeling in Large-Scale PV Power Plants," *Applied Energy* 384 (2025): 125423, https://doi.org/10.1016/j.apenergy.2025.125423.

6. H. Mao, W. Liu, C. Li, et al., "An Accurate Quantification Study on the Rooftop PV Potential Based UAV Field Photography in Dense Urban Environments," *Applied Energy* 399 (2025): 126499, https://doi.org/10.1016/j.apenergy.2025.126499.

7. Y. Tan, J. Peng, Z. Luo, et al., "Multi-Function Partitioned Design Method for Photovoltaic Curtain Wall Integrated with Vacuum Glazing towards Zero-Energy Buildings," *Renewable Energy* 218 (2023): 119257, https://doi.org/10.1016/j.renene.2023.119257.

8. W. Xiong, X. Deng, Z. Liu, R. Liu, Z. Wu, and L. Zhang, "Sustainability and Efficient use of Building-Integrated Photovoltaic Curtain Wall Array (BI-PVCWA) Systems in Building Complex Scenarios," *Energy and Buildings* 276 (2022): 112477, https://doi.org/10.1016/j.enbuild.2022.112477.

9. W. Jiang, T. Wang, D. Yuan, et al., "Available Solar Resources and Photovoltaic System Planning Strategy for Highway," *Renewable and Sustainable Energy Reviews* 203 (2024): 114765, https://doi.org/10.1016/j.rser.2024.114765.

10. National Energy Administration of China, *Photovoltaic Power Generation Construction in the First Half of 2024*, (2024), accessed 25 July 2024, https://www.nea.gov.cn/2024-07/25/c_1310782757.htm.

11. D. Bernadette, M. Twizerimana, A. Bakundukize, B. J. Pierre, and N. Theoneste, "Analysis of Shading Effects in Solar PV System," *International Journal of Sustainable and Green Energy*, 2 (2021): 47–62, https://doi.org/10.11648/j.ijrse.20211002.13.

12. D. Zhu, D. Wang, F. Wang, X. Gong, G. Yang, and R. Yan, "Experimental Study of the Effect of Fallen Leaf Shading on the Polarization Characteristics of Photovoltaic Modules," *SN Applied Sciences* 6 (2023): 165, https://doi.org/10.1007/s42452-023-05391-y.

13. A. K. Sisodia and R. Mathur, "Performance Enhancement of Solar Photovoltaic (PV) Module Using a Novel Flat Plate (NFP) Glass Cover by Reducing the Effect of Bird Dropping (BD) Settlement," *Environmental Science and Pollution Research* 4 (2022): 6104–6124, https://doi.org/10.1007/s11356-021-16082-9.

14. Å.F. Skomedal, B. L. Aarseth, H. Haug, J. Selj, and E. S. Marstein, "How much Power Is Lost in a Hot-Spot? A Case Study Quantifying the Effect of Thermal Anomalies in Two Utility Scale PV Power Plants," *Solar Energy* 211 (2020): 1255–1262, https://doi.org/10.1016/j.solener.2020.10.065.

15. A. Wang and Y. Xuan, "Close Examination of Localized Hot Spots Within Photovoltaic Modules," *Energy Conversion and Management* 234 (2021): 113959, https://doi.org/10.1016/j.enconman.2021.113959.

16. A. Pandian, K. Bansal, D. J. Thiruvadigal, and S. Sakthivel, "Fire Hazards and Overheating Caused by Shading Faults on Photo Voltaic Solar Panel," *Fire Technology* 2 (2016): 349–364, https://doi.org/10.1007/s10694-015-0509-7.

17. M. C. Alonso-Garcia, J. M. Ruiz, and F. Chenlo, "Experimental Study of Mismatch and Shading Effects in the I-V Characteristic of a Photovoltaic Module," *Solar Energy Materials and Solar Cells* 3 (2006): 329–340, https://doi.org/10.1016/j.solmat.2005.04.022.

18. A. Dolara, G. C. Lazaroiu, S. Leva, and G. Manzolini, "Experimental Investigation of Partial Shading Scenarios on PV (photovoltaic) Modules," *Energy* 55 (2013): 466–475, https://doi.org/10.1016/j.energy.2013.04.009.

19. V. Quaschning and R. Hanitsch, "Numerical Simulation of Current-Voltage Characteristics of Photovoltaic Systems with Shaded Solar Cells," *Solar Energy* 6 (1996): 513–520, https://doi.org/10.1016/0038-092X(96)00006-0.

20. D. A. Neamen, Chapter 7-the Pn Junction, in *Semiconductor Physics and Devices*, eds. P. E. Massar, (McGraw-Hill higher education, 2011)., 4th ed. ISBN: 978-0-07-352958-5.

21. Z. Xu, "Influence of Electron Irradiation on Backward Breakdown Voltage of Semiconductor Devices," *Nuclear Techniques* 14 (1991): 253–255.

22. Y. Li, Z. Liu, D. Liu, et al., "The Mechanism of the Semi-Transparent Coverings Affecting the Power Generation Capacity of the Photovoltaic Module and Array," *Energies* 7 (2024): 1601, https://doi.org/10.3390/en17071601.